(2)

AFATL-TP-88-131

Efficiency Scaling for Railgun Armatures

Lindsey Thornhill
Jad Batteh
Donald Littrell

SCIENCE APPLICATIONS INTERNATIONAL CORPORATION
1519 JOHNSON FERRY ROAD
SUITE 300
MARIETTA, GA 30062

DECEMBER 1988

FINAL REPORT FOR PERIOD OCTOBER 1987 - SEPTEMBER 1988

AIR FORCE ARMAMENT LABORATORY
Air Force Systems Command ▮ United States Air Force ▮ Eglin Air Force Base, Florida

Unclassified
SECURITY CLASSIFICATION OF THIS PAGE

REPORT DOCUMENTATION PAGE

Form Approved
OMB No 0704-0188
Exp Date: Jun 30, 1986

1a. REPORT SECURITY CLASSIFICATION Unclassified	1b. RESTRICTIVE MARKINGS
2a. SECURITY CLASSIFICATION AUTHORITY	3. DISTRIBUTION/AVAILABILITY OF REPORT Approved for Public Release; distribution is unlimited.
2b. DECLASSIFICATION/DOWNGRADING SCHEDULE	
4. PERFORMING ORGANIZATION REPORT NUMBER(S)	5. MONITORING ORGANIZATION REPORT NUMBER(S) AFATL-TP-88-131
6a. NAME OF PERFORMING ORGANIZATION Science Applications International Corporation 6b. OFFICE SYMBOL (If applicable)	7a. NAME OF MONITORING ORGANIZATION Electromagnetic Launcher Technology Branch Analysis & Strategic Defense Division
6c. ADDRESS (City, State, and ZIP Code) 1519 Johnson Ferry Road Suite 300 Marietta, GA 30062	7b. ADDRESS (City, State, and ZIP Code) Air Force Armament Laboratory Eglin Air Force Base, FL 32542-5434
8a. NAME OF FUNDING/SPONSORING ORGANIZATION Analysis & Strategic Defense Division 8b. OFFICE SYMBOL (If applicable) AFATL/SAH	9. PROCUREMENT INSTRUMENT IDENTIFICATION NUMBER F08635-87-C-0003
8c. ADDRESS (City, State, and ZIP Code) Air Force Armament Laboratory Eglin Air Force Base, FL 32542-5434	10. SOURCE OF FUNDING NUMBERS PROGRAM ELEMENT NO.: 63222C PROJECT NO: KEWA TASK NO.: G4 WORK UNIT ACCESSION NO: 33

11. TITLE (Include Security Classification)
Efficiency Scaling for Railgun Armatures

12. PERSONAL AUTHOR(S)
Lindsey Thornhill, Jad Batteh, Donald Littrell

13a. TYPE OF REPORT	13b. TIME COVERED	14. DATE OF REPORT (Year, Month, Day)	15. PAGE COUNT
Final	FROM Oct 87 TO Sep 88	December 1988	57

16. SUPPLEMENTARY NOTATION
Availability of this report is specified on verso of front cover.

17. COSATI CODES			18. SUBJECT TERMS (Continue on reverse if necessary and identify by block number)
FIELD	GROUP	SUB-GROUP	Railgun, Electromagnetic Propulsion, Electromagnetic Acceleration, Armature, Armature Efficiency, Plasma, Hybrid, Transitioning

19. ABSTRACT (Continue on reverse if necessary and identify by block number)

The results of a numerical study on three hypervelocity railgun armature options are presented in this paper. The armatures considered are the plasma, the hybrid, and the transitioning armatures. Several scaling studies are presented which illustrate the sensitivity of armature performance to variations in various railgun parameters. Armature performance scaling with projectile velocity, bore size (projectile mass), and current per unit rail height are all examined. An interesting conclusion of these studies is that armature efficiency tends to improve with increasing bore size. Also, results are presented from studies which determine how armature performance scales with uncertain parameters such as the ablation entrainment fraction, the skin friction coefficient, and the contact potential. These studies indicate which parameters have the greatest impact on armature performance and, therefore, need to be determined more accurately to predict railgun performance.

20. DISTRIBUTION/AVAILABILITY OF ABSTRACT ☐ UNCLASSIFIED/UNLIMITED ☒ SAME AS RPT ☐ DTIC USERS	21. ABSTRACT SECURITY CLASSIFICATION Unclassified
22a. NAME OF RESPONSIBLE INDIVIDUAL Donald M. Littrell	22b. TELEPHONE (Include Area Code) (904) 883-0398 22c. OFFICE SYMBOL AFATL/SAH

DD FORM 1473, 84 MAR — 83 APR edition may be used until exhausted. All other editions are obsolete

SECURITY CLASSIFICATION OF THIS PAGE
Unclassified

PREFACE

This report describes a joint effort conducted by personnel of Science Applications International Corporation (SAIC) and the Air Force Armament Laboratory (AFATL). This work was performed during the period 1 October 1987 to 30 September 1988 under contract F08635-87-C-0003 and was funded by the Electromagnetic Launcher Technology Branch (SAH), Strategic Defense and Analysis Division, AFATL, Eglin Air Force Base, Florida, under the Kinetic Energy Weapons program of the Strategic Defense Initiative.

The authors would like to acknowledge the very helpful suggestions of Capt. James Scanlon, Mr. Ken Cobb, and Dr. Joshua Kolawole.

TABLE OF CONTENTS

Section	Title	Page
I	INTRODUCTION	1
II	MODEL DEVELOPMENT	4
III	RESULTS	11
	1. Performance Scaling with Projectile Mass	11
	2. Performance Scaling with Current per Unit Rail Height	21
IV	SENSITIVITY STUDIES	25
V	CONCLUSIONS	31
Appendix		
A	DERIVATION OF THERMAL CONDUCTION PARAMETERS FOR ABLATION DRAG AND GAP GROWTH	35
B	DERIVATION OF PARASITIC MASS FOR HYBRID ARMATURES	41
C	ANALYTIC SOLUTION FOR ARMATURE EFFICIENCY	45
	REFERENCES	

LIST OF FIGURES

Figure	Title	Page
1	Armature Options	2
2	Armature Efficiency as a Function of Projectile Exit Velocity, (a) One-centimeter-bore, 2.5-gram Projectile (b) Ten-centimeter-bore, 2.5-kilogram Projectile	14
3	Variation of Armature Efficiency With Projectile Mass	20
4	Variation of Maximum Velocity With Current per Unit Rail Height for (a) the One-centimeter-bore and (b) the Ten-centimeter-bore Gun	22
5	Variation of Armature Efficiency With Current per Unit Rail Height for (a) the One-centimeter-bore and (b) the Ten-centimeter-bore Gun	24
6	Maximum Velocity as a Function of the Entrainment Fraction for the Transitioning Armature	26
7	Maximum Velocity as a Function of the Skin Friction Coefficient for the Transitioning Armature	27
8	Comparison of Voltage Scaling Relationships	29
9	Effect of Voltage Scaling on Armature Efficiency for (a) Hybrid and (b) Transitioning Armatures	30
10	Maximum Velocity and Efficiency for a Transitioning Armature Accelerating a 250-gram Projectile in a 10-cm Bore Gun	33

LIST OF TABLES

Table	Title	Page
1	Parameters for Calculating Armature Efficiency	12

SECTION I
INTRODUCTION

The armature is one of the key components of a railgun system since it serves as the medium whereby electrical energy delivered by the power supply is converted into projectile kinetic energy. The efficiency with which this conversion is accomplished is an important consideration in the assessment of railgun systems because it directly influences the requirements placed on the prime power and power conditioning components. Several mechanisms such as armature parasitic mass, armature resistance, viscous drag between the armature and the bore, and ablation of bore materials and entrainment of those materials into the armature (commonly referred to as ablation drag) can all have a deleterious effect on the armature efficiency. In addition, two of these loss mechanisms, viscous drag and ablation drag, impose a limit on the maximum velocity that can be achieved. The principal purpose of this paper is to develop a methodology for examining how armature efficiency and velocity limits scale with key gun performance parameters--such as projectile mass, bore size, and gun current per unit rail height--and to apply that methodology to the various hypervelocity armature concepts. (In this paper, the term hypervelocity is used to denote velocities in excess of 7 km/s.)

Our analyses are focused on only three of the four commonly used armature concepts, shown in Figure 1, since it is generally believed that the solid armature, which relies on solid-to-solid contact for current transfer to and from the rails, is limited, because of bore gouging and because of the difficulty of maintaining solid contact at high velocities, to a maximum velocity in the range of 3 to 5 km/s. In the plasma armature, current transfer is achieved through a moderate temperature, high-pressure arc which is typically several centimeters or 10's of centimeters long. The hybrid and the transitioning armatures are actually variations on the more basic designs of the solid and the plasma armatures. The hybrid armature consists of a solid conductor with plasma brushes bridging a small gap between the solid conductor and the rails. Its design is intended to overcome the velocity limitations on solid-to-solid contacts while preserving some of the advantages of the solid armature. The transitioning armature begins as a solid armature and transitions, after accelerating over several 10's of centimeters of bore, to a plasma armature as a

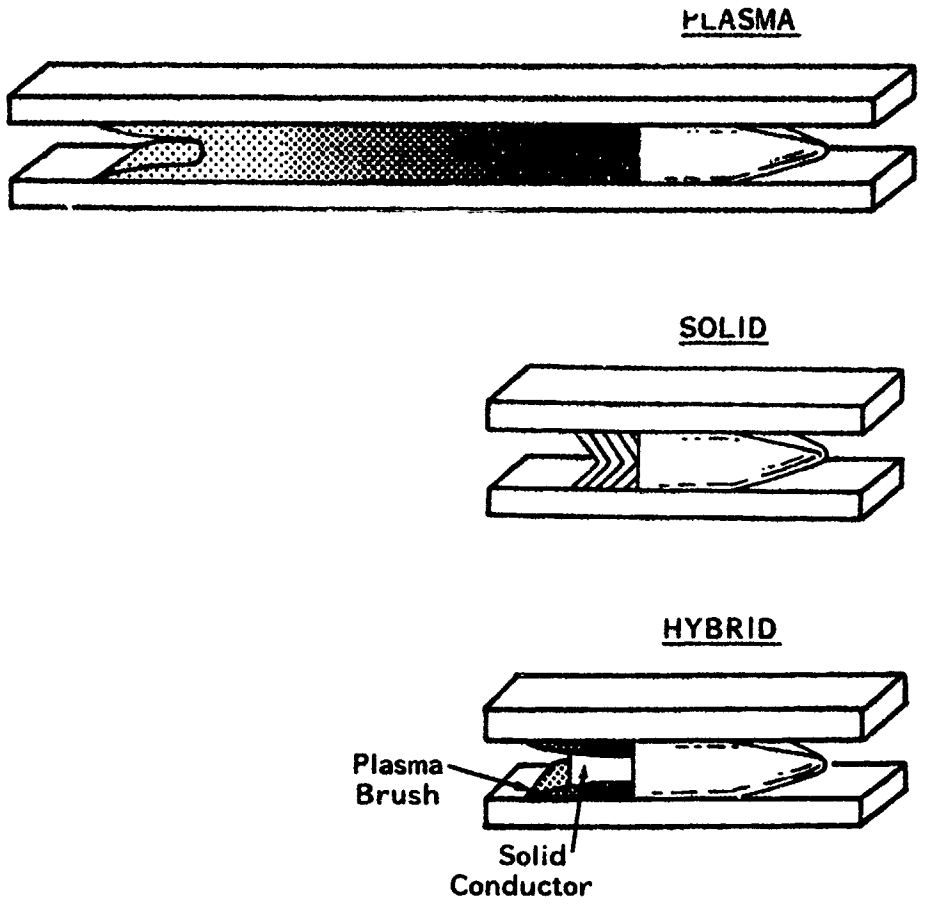

TRANSITIONING ARMATURE

Solid at Low Velocities
Transitioning to a
Plasma at High Velocities

Figure 1. Armature Options

result of ohmic heating. The intent of the transitioning armature is to eliminate plasma heating of the bore near the breech where it is most severe, because of the long transit time. The relative advantages and disadvantages of the four armature types have been discussed in detail in Reference 1.

Our analysis is based on the simultaneous solution of Newton's Law for the launch package (armature plus projectile) and equations which describe the ablation and entrainment of bore materials. To simplify the model, we consider a square-bore, constant-current, simple railgun. We are forced to make assumptions concerning the values of some parameters, particularly those related to viscous drag, ablation drag, and armature potential drop, because the magnitudes and scaling laws for these parameters are, at present, not well known. Therefore, we also report the results of calculations we have performed to determine how sensitive the trends predicted by the model are to uncertainties in several of the key parameters. These sensitivity studies are useful in determining which parameters appear to be most important in defining armature performance scaling, and serve as a guide to how experimental efforts might be focused to enhance our understanding of hypervelocity armatures.

The remainder of this paper is divided into four sections. Section II describes the development of the mathematical model for predicting armature efficiency. Section III contains the results of our scaling calculations for the plasma, hybrid, and transitioning armatures. Section IV describes the sensitivity calculations and Section V discusses the conclusions and recommendations.

SECTION II
MODEL DEVELOPMENT

To examine how armature performance scales with gun operating conditions, we employ a model, described in Reference 1, which computes the armature efficiency for a simple, square-bore, constant-current railgun. Since the model has been discussed elsewhere, we will only outline the defining equations here, except that we will provide a more extensive discussion of the formulation of the ablation drag term which differs somewhat from that used in Reference 1. The description of the model will focus primarily on plasma and hybrid armatures. The transitioning armature will be modeled simply as a solid armature which transitions instantaneously to a plasma armature at a specified velocity with no loss in energy.

For both hybrid and plasma armatures, the increase in velocity, v, of the projectile/armature system with time, t, is described by Newton's Law which we write as

$$(M_{sa} + M_{pa} + M_p)\frac{dv}{dt} = \frac{L'I^2}{2} - v\frac{dM_{pa}}{dt} - F_D. \qquad (1)$$

Here, M_{sa} is the mass of that portion of the armature which is in the solid state, M_{pa} is the mass of that portion in the plasma state, M_p is the projectile mass, L' is the gun inductance gradient, I is the gun current, and F_D is the drag force resulting from the armature/bore interaction. The first term on the right hand side represents the Lorentz force which accelerates the launch package, while the second and third terms represent the decrements in acceleration arising from ablation drag and the drag force between the armature and bore, respectively.

We assume that only the bore area wetted by the plasma portion of the armature contributes to the drag force, which we write as

$$F_D = \frac{2C_f M_{pa} v^2}{h}\left\{\frac{1 + 2\delta/h}{4\delta/h}\right\} \qquad (2)$$

where C_f is the skin friction coefficient for the plasma, h is the bore dimension, and δ represents the thickness of the gap between the solid conductor and

the rail. In the case of a plasma armature $\delta = \frac{1}{2}h$.

To calculate the ablation drag term in Equation (1) for the plasma armature, we assume that all the energy generated in the armature through ohmic dissipation and by friction is radiated uniformly to the bore. The following equation, based on an extension of the model proposed by Parker, et al., Reference 2, is then used to determine the change of the plasma mass with time:

$$\frac{dM_{pa}}{dt} = f_R \epsilon_R \beta_R Q_R + f_D \epsilon_D \beta_D Q_D \tag{3}$$

where Q_R and Q_D, given by

$$Q_R = Q_D = \frac{IV + vF_D}{2 + (h/\ell)} , \tag{4}$$

represent the heat flux to the rails and dielectrics, respectively. Here, V is the resistive voltage drop across the armature, ℓ is the armature length, and ϵ_R, the rail ablation coefficient, represents the mass of rail material which is vaporized, ionized, and raised to the arc temperature for a unit input of energy. The parameter β_R accounts for the fact that only a fraction of the energy incident on the rails leads to ablation, the remainder being expended in raising the surface temperature of the rails to the vaporization temperature or lost to thermal conduction into the rails. In Appendix A, we derive an expression for β_R as a function of the heat flux to the rail, the rail thermophysical properties, the projectile velocity, and the armature length. In writing Equation (3), we have assumed that only a fraction, f_R, of the mass ablated from the rail is actually entrained in the plasma armature. The variables with the subscript "D" refer to the corresponding parameters for the dielectrics.

Our ablation model differs from that of Reference 2 in two respects. First, our formulations for β_R and β_D account explicitly for the energy expended in raising the bore surface to its vapor temperature and for the energy conducted into the bore. Second, we have included frictional heating of the plasma armature, in addition to ohmic dissipation, as a second source of thermal energy which is eventually transferred to the bore.

The voltage drop in Equation (5) is assumed to be the sum of a net contact potential per anode/cathode pair, V_c, and a bulk voltage drop which scales with bore dimension. Consequently, for the plasma armature the voltage drop is

written as

$$V = V_c + V_b' h^{\alpha} \quad . \tag{5}$$

Because of the limited data for bore sizes beyond a few centimeters, there is considerable uncertainty in the evaluation of the parameters in Equation (5). For the set of baseline calculations presented here, we use $V_c = 100$ V based on the experiments of Jamison Reference 3. Muzzle voltages obtained from experiments with small-bore guns, Reference 4, and with the Maxwell Single Shot Gun (SSG) Refernce 5, suggest voltage drops of approximately 155 V and 350 V in bores of the order of 1 cm and 10 cm, respectively. With 100 V for the contact potential, we can use the small-bore and SSG data to determine α and V_b', with the result that $\alpha = 0.658$, and $V_b' = 1138$ V/(m^{α}).

The form of Equation (5) does not allow an explicit dependence of armature voltage on current. There is, of course, an implied dependence that guns with larger bores typically operate at higher currents. Unfortunately, the experimental data currently available does not allow a distinction between the effect of a change in current and a change in bore dimension. Therefore, we have chosen to use Equation (5) until experiments are performed to separate the two contributions.

The armature length, ℓ, which appears in the calculation of β_R and β_D is assumed to scale with the number of heavy particles in the plasma according to the relation

$$\ell = \ell_i \left\{ \frac{M_{pa}}{M} \frac{\bar{M}_i}{M_{pai}} \right\} \quad . \tag{6}$$

The average molecular weight of the armature, $\bar{M}$, is allowed to change with time due to the entrainment of rail and dielectric materials, and the subscript "i" in this expression denotes values at t=0.

Since there is no direct measurement of plasma armature mass in railgun experiments, we base our estimate for M_{pai} on analysis of experimental data. Calculations, Reference 6, for the Rashleigh-Marshall experiment suggest a plasma armature mass to projectile mass ratio of 0.053. Studies, References 7, 8, and 9, of data taken from CHECMATE suggest values for this ratio of 0.035 to 0.061 if the major constituent of the armature is assumed to be copper. Based on these calculations, we assume that the initial mass of the plasma armature

is related simply to the projectile mass by the expression

$$M_{pai} = 0.05M_p \ . \tag{7}$$

To estimate the initial armature length, we assume that the plasma armature temperature and degree of ionization are independent of gun operating conditions so that the average density in the plasma is directly proportional to the pressure. Equating the pressure to the Lorentz force per unit bore area, the average density of the plasma armature can be written as

$$\rho_{pa} = Kj^2 \tag{8}$$

where j is the current per unit rail height and K is a constant. Once again, the value of 3×10^{-14} kg/A^2m, used in this study for K, is based on analyses, References 6 through 9 of the Rashleigh-Marshall experiments and the CHECMATE experiments, which suggest values in the range from 2×10^{-14} to 3×10^{-14} kg/A^2m. Combining Eqs. (7) and (8) allows us to estimate an initial armature length, ℓ_i.

The entrainment fractions, f_R and f_D, are likely to be complicated functions of the geometry and composition of both the armature and the bore, the armature radiative properties, and the armature velocity. Since the details of these various functional dependencies are, at present, unclear, we have made rather simplistic assumptions regarding the values of the entrainment fractions in Section III in order to illustrate the potential impact of ablation drag on performance.

The effect of ablation drag on the performance of the hybrid armature is neglected in our calculations since experimental evidence to date, albeit limited, suggests that for $\delta/h \ll 1$, there is negligible entrainment of material ablated from the rails and insulators into the plasma brushes, Reference 10. Therefore, Equation (3) is not required for the analysis of the hybrid armature. However, an additional equation must be solved which describes the growth of the gap between the solid armature and the rails arising from ablation of the solid armature. The increase in δ leads to an increase in the armature voltage drop and in the losses due to frictional interaction with the insulators, and a decrease in the armature mass. To calculate the increase in

δ we assume that the energy generated by ohmic dissipation in the plasma brushes and by viscous interaction with the bore is radiated uniformly from the surface of the plasma brushes. Furthermore, we assume that the solid armature constrains the plasma brush such that its length, ℓ, is equal to the length of the solid armature, ℓ_s. The equation for the gap growth can then be written as

$$\frac{d\delta}{dt} = \left\{ \frac{IV + vF_D}{2} \right\} \frac{\beta_s \varepsilon_s}{2\rho_s(\ell_s h + \delta h + \delta \ell_s)}, \tag{9}$$

where ρ_s is the effective density of the solid armature and ε_s is the appropriate ablation coefficient for the solid armature. An expression for β_s, which represents the fraction of the heat flux to the solid armature which actually leads to ablation, is derived in Appendix A. The mass of the plasma brushes is determined from

$$M_{pa} = 2\rho_{pa}\delta\ell_s h \tag{10}$$

where the density of the plasma brush, ρ_{pa}, is assumed to be given by Equation (8). The mass of the solid conductor in the hybrid varies as

$$M_{sa} = M_{sai} \frac{1 - 2\delta}{1 - 2\delta_i} \tag{11}$$

where δ_i is the initial value of the gap dimension, and M_{sai} is the initial mass of the solid conductor. As discussed in Appendix B, M_{sai} is calculated based on the action of the solid conductor and the total acceleration time, t_f, with the result that

$$M_{sai} = f_{ac} h I \left\{ \frac{t_f}{\gamma} \right\}^{1/2}. \tag{12}$$

In Equation (12),

$$\gamma = \frac{1}{\rho_s} \int_{T_i}^{T_f} \frac{C_p}{\eta_r} dT \tag{13}$$

where C_p is the specific heat of the solid conductor, η_r its resistivity, T_i its initial temperature, and T_f the allowed final temperature of the armature

material. f_{ac} represents the ratio of the total armature mass to the conductor mass and is used to allow for the possibility that the solid conductor may be imbedded in a nonconducting matrix to provide a more uniform distribution of current in the armature.

In the hybrid armature, the voltage drop across the solid armature is neglected relative to the drop across the plasma brushes. The voltage drop across each brush is assumed to obey the same scaling as the plasma armature, so that the voltage drop across the hybrid armature is given by

$$V = 2(V_c + V_b' \delta^{\alpha}) \quad . \tag{14}$$

Equations (1) and (3) or (1) and (9) are solved for the plasma or hybrid armature, respectively. For the transitioning armature, only losses associated with parasitic mass and resistive voltage drop are considered when the armature is in the solid state. Frictional effects are neglected since transition takes place at relatively low velocities where drag is not dominant. Also, bore ablation is neglected while the armature is in the solid state since we have assumed the ohmic energy is absorbed by the solid armature. The armature is assumed to transition with no loss in energy and at transition it is given the characteristics of a plasma armature at the corresponding gun operating conditions.

For the purpose of comparing various armature types we define an armature efficiency, η, as the ratio of the increase in projectile kinetic energy to the energy provided to the armature to accelerate the armature/projectile system to velocity v. The armature efficiency, as defined, may be written as

$$\eta = \frac{M_p (v^2 - v_i^2)}{2 \int_o^t (IV + \tfrac{1}{2} L' I^2 v) dt} \tag{15}$$

where t is the time required to accelerate the armature/projectile system to velocity v.

In Appendix C an analytical expression is derived for the armature efficiency in the limit where the dominant loss mechanisms are the initial parasitic mass of the armature and armature voltage drop. This expression is valid for the transitioning armature prior to transition and, as we shall see

in Section III, provides a good approximation for the efficiency of hybrid armatures.

SECTION III
RESULTS

1. PERFORMANCE SCALING WITH PROJECTILE MASS

In this section, we assess the relative importance of the various loss mechanisms for plasma, hybrid, and transitioning armatures, and determine how armature performance scales with projectile mass. As projectile mass is increased, we assume that the density of the projectile and its ratio of length to transverse dimension are held fixed, and that the current per unit rail height, j, is held constant. Consequently the bore dimension and gun current scale as

$$h = C_h M_p^{1/3} \tag{16}$$

$$I = jh \ . \tag{17}$$

For the calculations presented in this section, we take C_h to be 0.074 $m/kg^{1/3}$ and j equal to 3×10^7 A/m. Throughout the remainder of this paper we refer to scaling with bore size and scaling with projectile mass interchangeably.

Other parameters used in the calculations presented here are listed in Table 1. The value for the skin friction coefficient was chosen from the range of values established by Parker et al., Reference 2. We have taken the rail material to be copper, the initial armature material to be aluminum, and the insulators to be polyethylene. This choice of materials establishes the material properties listed in Table 1 (i.e. ablation coefficients, atomic or molecular weights, vapor temperatures, thermal conductivities, thermal diffusivities, and solid armature density). The λ's in Table 1 are defined in Appendix A and are merely dimensionless combinations of thermal properties. γ, which is defined by equation (13), is a material property of the solid armature related to its action constant.

The gun inductance gradient is assumed to be 0.5 μH/m, a representative value for simple railguns. We have assumed, in addition, that there is no pre-injection (i.e. the projectile initial velocity is zero) which makes the results of our ablation studies conservative, since ablation effects could, presumably, be lessened by injecting the projectile with some initial velocity.

TABLE 1. PARAMETERS FOR CALCULATING ARMATURE EFFICIENCY

Parameter	Value	Units
C_F	2×10^{-3}	
ϵ_R	4.7×10^{-8}	kg/J
ϵ_D	4×10^{-9}	kg/J
ϵ_S	1.3×10^{-8}	kg/J
MW_1	26.98	g/mole
MW_R	63.54	g/mole
MW_D	4.67	g/mole
$T_{v,R}$	2830	K
$\bar{k}_R$	290	W/mK
$\bar{\alpha}_R$	7.9×10^{-5}	m^2/S
λ_R	0.287	
$T_{v,D}$	463	K
$\bar{k}_D$	0.3	W/mK
$\bar{\alpha}_D$	2.08×10^{-7}	m^2/S
λ_D	0.405	
$T_{v,S}$	2800	K
$\bar{k}_S$	238	W/mK
$\bar{\alpha}_S$	1×10^{-4}	m^2/S
ρ_S	2700	kg/m^3
γ	4.3×10^9	m^2A^2S/kg^2

Another factor which tends to make our estimates of ablation effects conservative is our assumption that the ablation entrainment fractions, f_R and f_D, are unity. We assume the initial gap width in the hybrid armature to be 1 mm for both the 1 cm bore gun and the 10 cm bore gun, and we take the ratio of the solid armature mass to conductor mass, f_{ac}, to be 1.5. For the transitioning armature, we transition the armature from solid to plasma when the armature/projectile velocity reaches 3 km/s.

In Figure 2a we show three sets of armature efficiency versus projectile velocity curves for a one-centimeter-bore railgun accelerating a 2.5-gram projectile to velocities up to 15 km/s. The three sets correspond to the calculations for a plasma, hybrid, and transitioning armature. The trends exhibited by these curves were discussed in detail in a previous publication, Reference 1. The objective here is to investigate how armature efficiency scales with projectile mass. Therefore, we have shown plotted, for comparison, in Figure 2b the corresponding curves for a ten-centimeter-bore railgun accelerating a 2.5-kilogram projectile.

Five separate calculations are shown for each armature type to help illustrate the importance of each loss mechanism and how these losses scale with projectile mass. The Case 1 calculations, indicated by a "1" following the curve, show the loss in efficiency associated only with the initial parasitic mass of the armature. In the Case 2 calculations, the losses due to armature resistance are included along with those resulting from the armature parasitic mass. Case 3 considers the effects of armature friction with the bore as well as the losses described for Cases 1 and 2. In Cases 4 and 5 we add the effects of ablation to the other loss mechanisms. Case 4 includes the effect of mass ablation arising from ohmic dissipation in the armature and Case 5 adds the effect of mass ablation arising from viscous heating in the armature. For the plasma and transitioning armatures, this means that mass is ablated from the bore and entrained in the plasma. For the hybrid armature, ablation refers to solid armature mass being ablated so that the brush gaps get wider.

The general trends exhibited by the net efficiency, Case 5, in Figure 2 are quite interesting. First we see that the efficiencies predicted for the small-bore gun are all quite low. In particular, we calculate values for η of 0.5 or less for the plasma and transitioning armatures, and 0.3 or less for the hybrid armature. Furthermore, the calculations indicate a maximum achievable

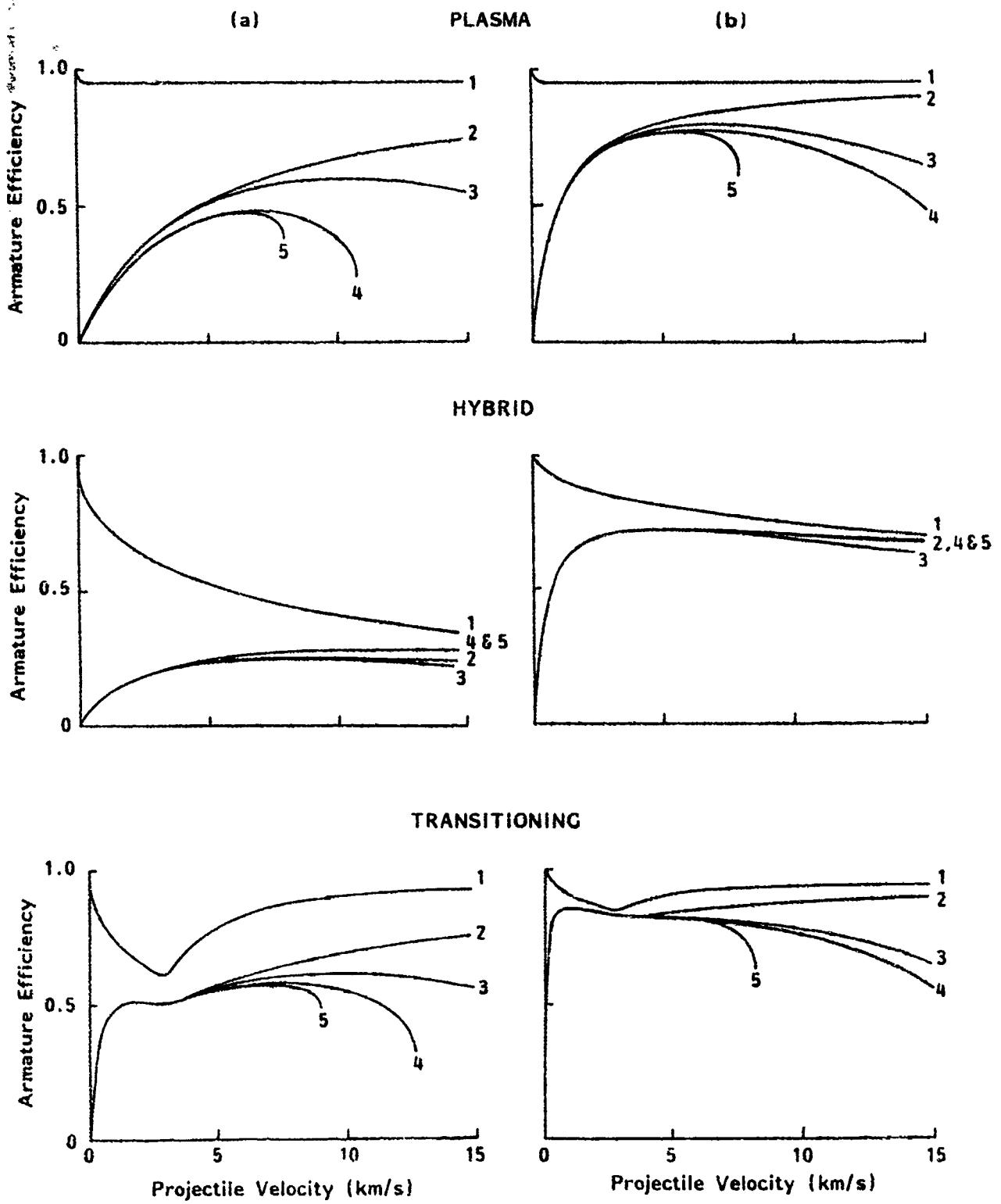

Figure 2. Armature Efficiency as a Function of Projectile Exit Velocity, (a) One-centimeter-bore, 2.5-gram Projectile (b) Ten-centimeter-bore, 2.5-kilogram Projectile

velocity, for the conditions studied here, of approximately 8 km/s for the small-bore plasma armature and 9 km/s for the small-bore transitioning armature. The calculations do not predict a velocity limit within the range studied here for the hybrid armature. Comparison of Figures 2a and 2b suggests a favorable scaling for armature efficiency with increasing projectile mass and bore size. In particular maximum efficiencies of 0.77, 0.73, and 0.87 are calculated for the plasma, hybrid, and transitioning armatures, respectively. Despite the improved efficiency, the maximum achievable velocities for the plasma and transitioning armatures are approximately the same for the large-bore calculations as for the small-bore calculations. The scaling of maximum velocity with bore size predicted by our calculations is less favorable than the scaling predicted by Parker et al., Reference 2, primarily because we include frictional heating of the plasma armature in calculating ablation drag.

Insight into the trends shown in Figure 2 can be obtained by considering the scaling of each loss mechanism with bore height. The armature efficiency may be determined analytically for Case 1. This efficiency is given by (see Appendix C)

$$\eta_1 = \left\{1 + \frac{M_{ai}}{M_p}\right\}^{-1} \tag{18}$$

where η_1 is the Case 1 efficiency and M_{ai}/M_p is the initial value of the ratio of the armature mass to the projectile mass. For the plasma armature, we have taken this mass ratio to be a constant, given by Equation (7). Therefore, the Case 1 efficiency for the plasma armature, in both the one-centimeter bore and the ten-centimeter bore, is equal to the constant value, 0.95.

For the hybrid armature, we see that the larger parasitic mass of the solid conductor causes the Case 1 armature efficiency to be considerably lower than for the plasma armature. As discussed in Appendix B, the solid mass of the hybrid armature must be sized to prevent melting during the acceleration time. An analytical expression may be derived for Case 1 solid armature mass as a function of bore size, final projectile velocity, v_f, projectile mass, inductance gradient, and the parameter, γ, (see Equation 13). This expression is given by

$$\frac{M_{sai}}{M_p} = \lambda \left[1 + (1 + 2/\lambda)^{\frac{1}{2}}\right] \tag{19}$$

where

$$\lambda = \frac{f_{ac}^2 \, h^2 \, (v_f - v_i)}{\gamma L' M_p} \quad . \tag{20}$$

It is interesting to note that the mass ratio given by Equation (18) is independent of gun current. Furthermore, since we have scaled the projectile mass as the cube of the bore dimension, one can see from Equation (20) that λ scales as 1/h. For large values of λ, the mass ratio in Equation (18) scales as 1/h, whereas for small values of λ, it scales as $1/h^{\frac{1}{2}}$. (Typical values for λ in our calculations range from 0.06 to 0.6.) In any case, the ratio M_{sai}/M_p decreases with increasing projectile mass. Therefore, we expect the losses associated with the large parasitic mass of the hybrid armature to be greater for small-bore guns than for large-bore guns at a given projectile velocity. This degradation in hybrid armature performance with smaller bore size is apparent in the armature efficiency curves in Figure 2.

In simulating the transitioning armature, we have assumed that the armature instantly transitions from a solid to a plasma when its velocity reaches 3 km/s. The decrease in transitioning armature efficiency at low velocities, seen in Figure 2, is a result of accelerating the solid armature mass to 3 km/s. This efficiency decrease is more pronounced in the one-centimeter gun than in the ten-centimeter gun for the reason described above; namely, the scaling of M_{sai}/M_p with h. After the armature transitions to the plasma state the Case 1 armature efficiency asymptotically approaches the 0.95 value found for the plasma armature.

The effects on armature performance of including armature resistance, the Case 2 calculations, are most pronounced in the plasma and hybrid armatures at low velocities. In the transitioning armature, the small resistance of the solid armature helps to negate the deleterious effects of armature resistance at velocities below 3 km/s. Once again, we can derive an analytical expression for the Case 2 armature efficiency (see Appendix C), namely

$$\eta_2 = \frac{1}{\left\{1 + \frac{M_a}{M_p}\right\} \, (1 + \mu)} \tag{21}$$

where

$$\mu = \frac{4V}{L'I(v_f + v_i)} \tag{22}$$

represents the decrement in armature efficiency arising from the voltage drop, V, in the armature.

For the plasma armature, M_a/M_p is a constant, since for Case 2 we are not yet considering ablation. According to Equation (5) V scales as h^α for large h, and I scales as h. Combining these scaling relationships with Equation (22) shows that μ for the plasma armature scales approximately as $h^{\alpha-1}$ for a given v_f and v_i. The parameter α was determined to be less than one, so increasing the bore size should decrease the impact of armature resistance on performance. This favorable scaling with increasing bore height is clearly visible in the plasma armature curves of Figure 2.

For the hybrid armature, the voltage drop is obtained from Equation (14) where the drop across the solid part of the armature has been neglected relative to the drop across the plasma brushes. The reduction in armature efficiency resulting from armature resistance is greater in the small-bore hybrid armature than in the small-bore plasma armature, because the hybrid armature has a net voltage drop which exceeds that of the plasma armature. Also, the scaling of M_a/M_p with h, as well as the scaling of V with h described for the plasma armature, lead to a scaling of Case 2 armature efficiency as $h^{2-\alpha}$ for the hybrid armature. This improvement in armature efficiency with larger bore size can be seen in Figure 2.

The small resistance of the transitioning armature in the solid phase greatly enhances the Case 2 efficiency of the armature at low velocities in comparison with the plasma and hybrid armatures. After the armature transitions to the plasma state, it behaves essentially as a plasma armature with all the scaling relationships developed for plasma armatures being applicable.

In the Case 3 calculations we have added the effects of friction between the armature and the bore. Introducing friction puts an upper bound on the maximum velocity that can be achieved for a given current. This velocity maximum may be determined by equating the Lorentz force to the drag force in Equation (1) to get

$$v_{max} = \left\{\frac{hL'}{4C_f M_{pa}}\right\}^{\frac{1}{2}} I \qquad (23)$$

for the plasma armature. Since the dependence on h cancels in Equation (23) both the one-centimeter bore and the ten-centimeter bore have the same maximum velocity, if ablation effects are neglected. For the parameters used to generate the curves in Figure 2, this maximum velocity is 21 km/s. The fact that the Lorentz force and the drag force scale equivalently (as h^2) suggests that frictional drag has approximately the same effect on performance in the large-bore gun as in the small-bore gun; this is evident in the Case 3 curves for the plasma armature in Figure 2.

Although the expression for the maximum velocity attainable with the hybrid armature is slightly more complicated than Equation (23), a scaling analysis leads to the same conclusion, i.e. the maximum velocity does not depend on h in the absence of ablation. (It should be mentioned that this conclusion is based on our assumption that the gap thickness, δ, is the same for both bore sizes.) Once again, in Figure 2, we see roughly the same relative degradation in efficiency from drag for the hybrid armature in both the large-bore and small- bore guns.

The Case 3 curves for the transitioning armature closely resemble those for the plasma armature. For these calculations we have assumed that the friction between the solid armature and the bore is negligible since the transition occurs at a relatively low velocity, 3 km/s. After transition, we find, as before, the scaling of the friction force to be balanced by an equivalent scaling of the Lorentz force.

The Case 4 curves in Figure 2 illustrate the potential impact of ablation due to ohmic dissipation in the armature. In the plasma and transitioning armatures, the effect of this ablation is to degrade armature performance because mass is entrained into the armature. The degradation in efficiency is much more severe in the one-centimeter gun than in the ten-centimeter gun because of the nonlinear scaling of the armature voltage drop described in Equation (5). Indeed, ablation drag, as modeled here, limits the maximum velocity which can be achieved in the small-bore gun to approximately 11 km/s for the plasma armature and 13 km/s for the transitioning armature.

For the hybrid armature, the addition of ablation resulting from ohmic dissipation is seen to improve armature performance in the Case 4 curves of Figure 2. This improvement in performance arises because the solid part of the armature is allowed to ablate while only enough mass is entrained in the plasma brushes to fill the increased gap. Therefore, the armature is becoming less massive as it accelerates. The effect is only slightly different in the two bore sizes because the armature voltage drop is dominated by the contact potential.

Finally, the results shown in the Case 5 curves of Figure 2 demonstrate the effects of ablation resulting from frictional heating of the armature. The armature efficiency curves for the plasma and transitioning armatures indicate that ablation from frictional heating plays a more dominant role in limiting the maximum velocity in the ten-centimeter gun, than in the one-centimeter gun. This difference in dominant ablation mechanisms is, once again, a result of the nonlinear scaling of the armature voltage drop with bore dimension. In particular, according to Equation (4), the ohmic contribution to the heat flux, for $h/\ell \ll 1$, increases at most as $h^{1+\alpha}$ whereas the contribution from friction, based on the initial armature mass, increases as h^2. In addition, there is a nonlinear effect in that mass entrainment increases the plasma armature mass and thereby increases the heating of the bore by friction. The effects of ablation due to frictional heating in the plasma brushes of the hybrid armature are not distinguishable from the effects of ohmic ablation at the velocities studied. The ohmic dissipation mechanism is clearly dominant in the hybrid armature.

In the remainder of this paper, the term armature efficiency will be used to denote the Case 5 calculation, that is the efficiency with all loss mechanisms included.

To further illustrate the sensitivity of armature efficiency to projectile mass, we show, in Figure 3, armature efficiency as a function of projectile mass for a muzzle velocity of 7.5 km/s. As indicated in the figure, the efficiencies of all three armature types display a trend which, in general, favors large projectile masses, although the curves for the plasma and transitioning armatures display a rather broad maximum for a projectile mass on the order of 6 kg.

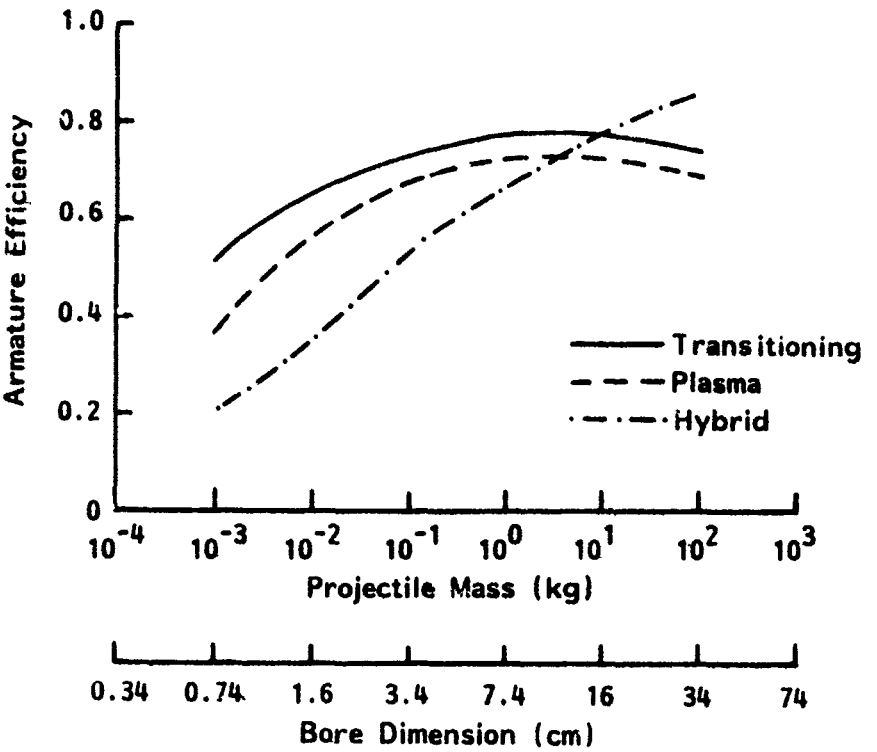

Figure 3. Variation of Armature Efficiency With Projectile Mass (v = 7.5 km/s)

2. PERFORMANCE SCALING WITH CURRENT PER UNIT RAIL HEIGHT

In this section we use our armature models to investigate how railgun performance is affected by changes in the current per unit rail height. First we examine the impact of varying j on the maximum obtainable velocity for the large-bore and small-bore simulations. These calculations were made for the plasma and transitioning armatures only, since the hybrid armature shows no velocity limit below 15 km/s. The results from this study on current scaling are shown in Figure 4.

Several limits exist to the maximum current allowable in a railgun. One limit is determined by the maximum current that the rails can carry before ohmic heating causes the rails to melt. Hawke, et al., Reference 11, finds this limit, for copper rails, to be $j_{max} = 4.3 \times 10^7$ A/m. Another limit on the maximum allowable current is determined by the maximum stress exerted on the rails before they yield. This current limit is estimated from the equation

$$j_{max} = \left[\frac{2\sigma_y}{L'}\right]^{1/2} \tag{24}$$

where σ_y is the compressive yielded strength of the rail material. For copper rails and an inductance gradient of 0.5 μH/m the current limit is given by $j \leq 3.5 \times 10^7$ A/m.

Finally, one other limit on the allowable current is derived from the maximum acceleration, A_{max}, the projectile can withstand:

$$j_{max} = \left[\frac{2A_{max}\, M_f}{L'\, h^2}\right] \tag{25}$$

Assuming $A_{max} = 10^7$ m/s^2, we find that for the 1 cm gun $j_{max} = 3.2 \times 10^7$ A/m and for the 10 cm gun $j_{max} = 10^8$ A/m.

In summary, thermal and mechanical considerations suggest a peak value of j in the range from 3.2×10^7 to 4.3×10^7 A/m. Therefore, in Figure 4, we have indicated a current per unit rail height of 4×10^7 A/m with a vertical line as a reference.

According to Equation (1), the velocity maximum is determined by the velocity at which the Lorentz force is balanced exactly by the viscous drag and ablation drag terms. At low values of j, viscous drag plays the dominant role

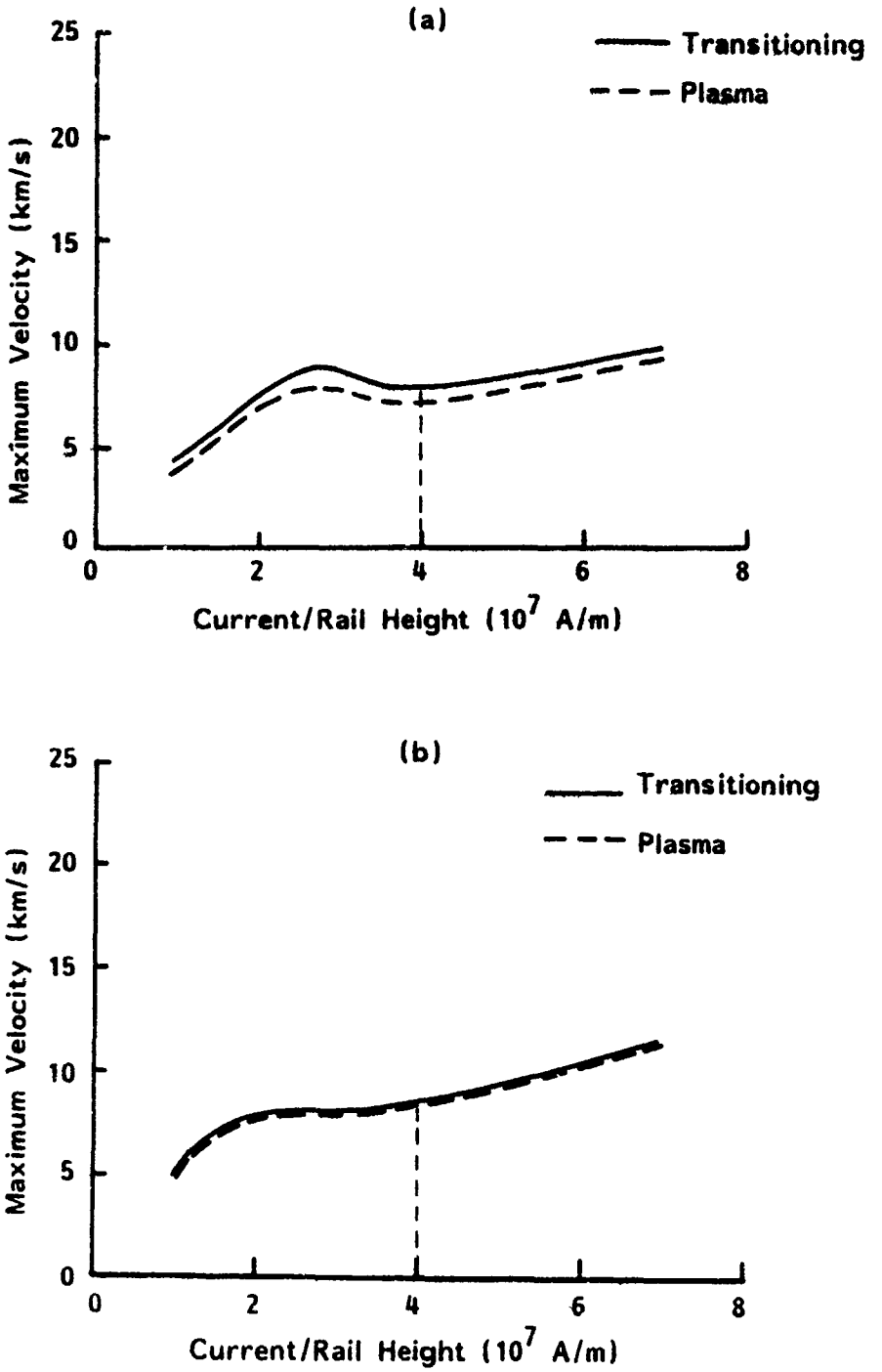

Figure 4. Variation of Maximum Velocity With Current per Unit Rail Height for (a) the One-centimeter-bore and (b) the Ten-centimeter-bore Gun

in balancing the Lorentz force, while at high values of j, the ablation drag term is more dominant. Both loss mechanisms are important in the range of about 3 to 4 x 10^7 A/m.

If we neglect ablation effects, increasing the current should always lead to an increase in v_{max}. In fact, Equation (1) indicates that

$$v_{max} = \left\{\frac{hL'}{4C_f M_{pa}}\right\}^{\frac{1}{2}} I \quad . \tag{26}$$

However, we must consider ablation effects and the impact of the change in current on ablation. Ablation leads to an increase in armature mass, and to the introduction of the dM_{pa}/dt term in Equation (1). This effect tends to decrease v_{max} below that predicted in the absence of ablation. The amount of the reduction in v_{max} as a function of I is quite complicated because of the impact of I on the ablation characteristics.

The current influences the amount of mass ablated in three ways, according to Equation (3). First, for a given velocity and armature voltage, the power dissipated in the armature, Q, increases as I increases. On the other hand, the acceleration time decreases, which tends to decrease the ablated mass. Finally, we find that, as current increases, the value of β, at a given velocity, increases. We now have two opposing trends – as current increases the energy dissipated in the armature and transferred to the bore during acceleration decreases but this energy is more effective in causing ablation. It is the relative importance of these two opposing trends that leads to the complex shape of the v_{max} versus I curve.

Figure 5 shows the efficiency at which a projectile can be accelerated to 7.5 km/s for a range of values of j for the three armature types. In general, we note that increasing j leads to an increase in η. The missing part of the small-bore plasma armature curve in Figure 5 means that the specified velocity, 7.5 km/s, could not be achieved in the corresponding current per unit rail height range.

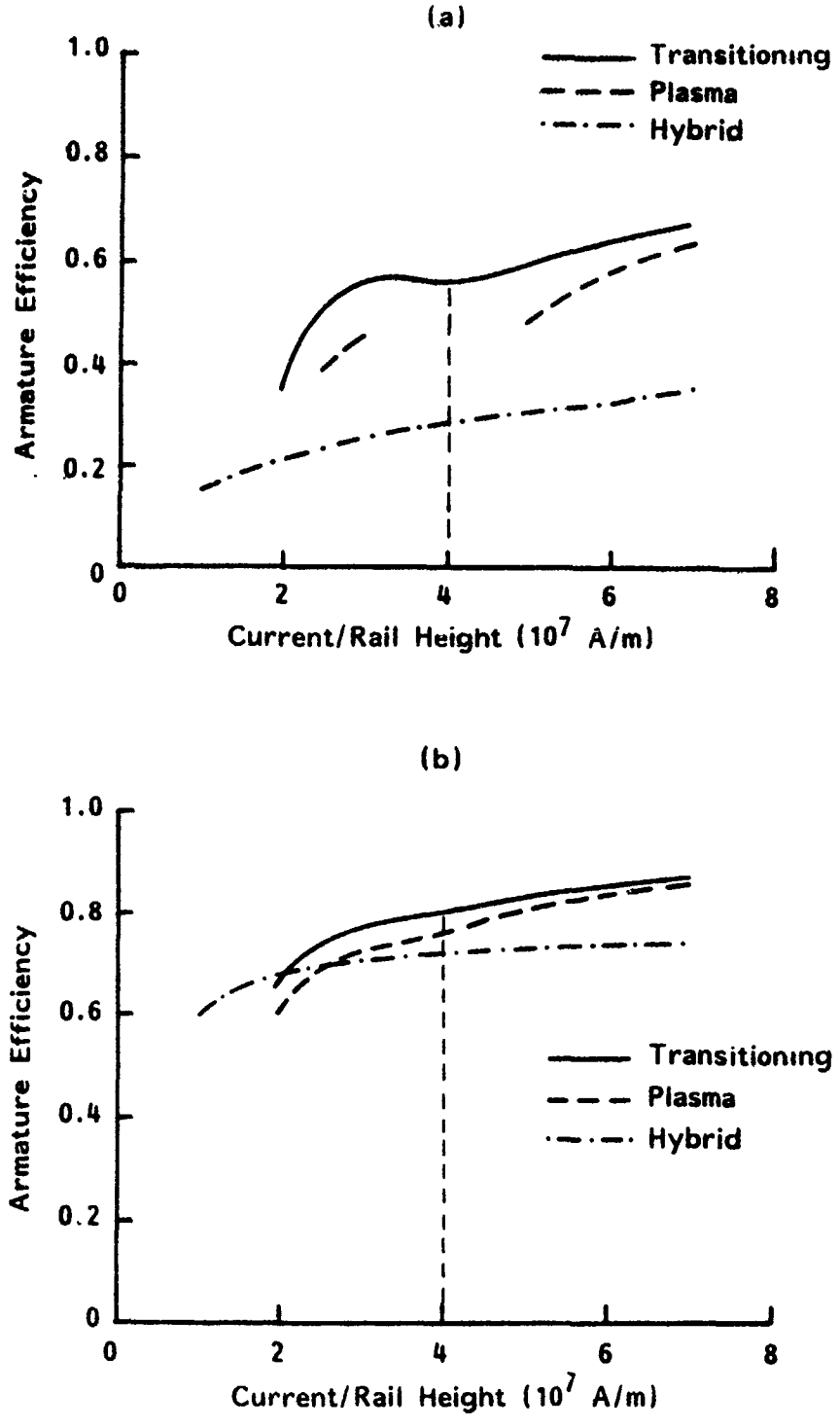

Figure 5. Variation of Armature Efficiency With Current per Unit Rail Height for (a) the One-centimeter-bore and (b) the Ten-centimeter-bore Gun (v ≈ 7.5 km/s)

SECTION IV
SENSITIVITY STUDIES

A number of the scaling parameters employed in calculating the armature efficiency are not well known. In this section, we focus on the sensitivity of our performance predictions to three of these parameters, namely the entrainment fraction, the friction coefficient, and the contact potential.

Two of the least understood parameters in our model of the armature are the entrainment fractions, f_R and f_D. The sensitivity of our results to the values used for these parameters is illustrated in Figure 6 where we have plotted curves of the maximum velocity attainable with a transitioning armature as a function of the entrainment fraction for both the large-bore and the small-bore gun. For these calculations, f_R and f_D were set equal. As the entrainment fraction is varied from 0 to 1, the maximum velocity decreases significantly from 21 km/s to less than 10 km/s, with the large-bore gun displaying slightly greater sensitivity. It is interesting to note, however, that the limiting velocity is relatively insensitive to the entrainment fraction for values of f greater than approximately 0.5.

Another parameter about which very little is known is the skin friction coefficient, C_f. The curves in Figure 7 give some indication of the sensitivity of our calculations to uncertainty in the value of C_f. Here we have plotted the maximum velocity as a function of the skin friction coefficient for values of C_f between 1×10^{-3} and 6×10^{-3}. It has been suggested that the value for C_f lies within this range, Reference 2. As indicated by the figure, the maximum velocity is very sensitive to C_f. For example, the small-bore velocity limit at $C_f = 1 \times 10^{-3}$ is about 11.5 km/s while at $C_f = 6 \times 10^{-3}$ the velocity limit is only 6 km/s, a reduction of 48 percent. Thus, uncertainty in the value of the skin friction coefficient has a significant impact on our ability to accurately predict armature performance.

There is, at present, no direct measurement of the contact potential at the solid/plasma interfaces in the armature. For the efficiency calculations described so far, a value of 100 V per anode/cathode pair was used, a value inferred from limited experimental measurements, Reference 3. Contact potentials derived from experiments and modeling in arc discharges, albeit at much lower pressures and currents, are considerably lower, generally falling

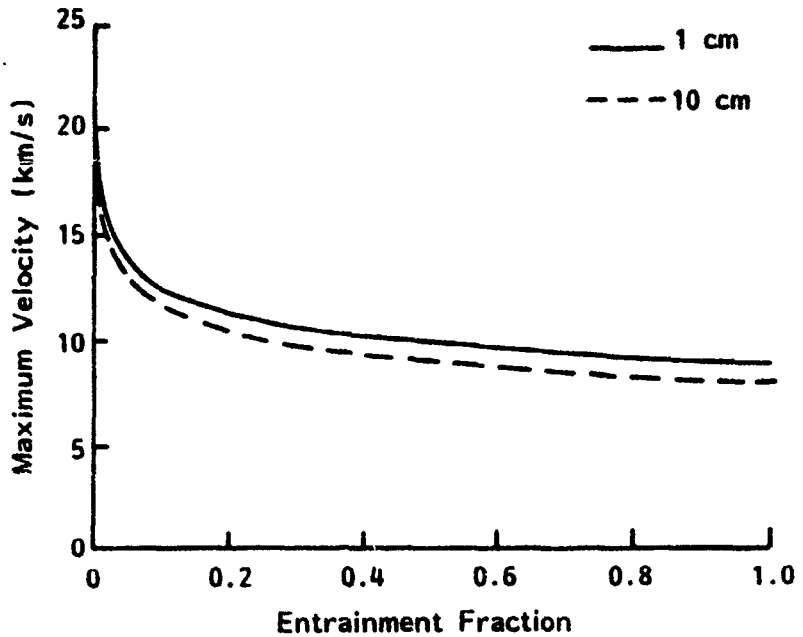

Figure 6. Maximum Velocity as a Function of the Entrainment Fraction for the Transitioning Armature

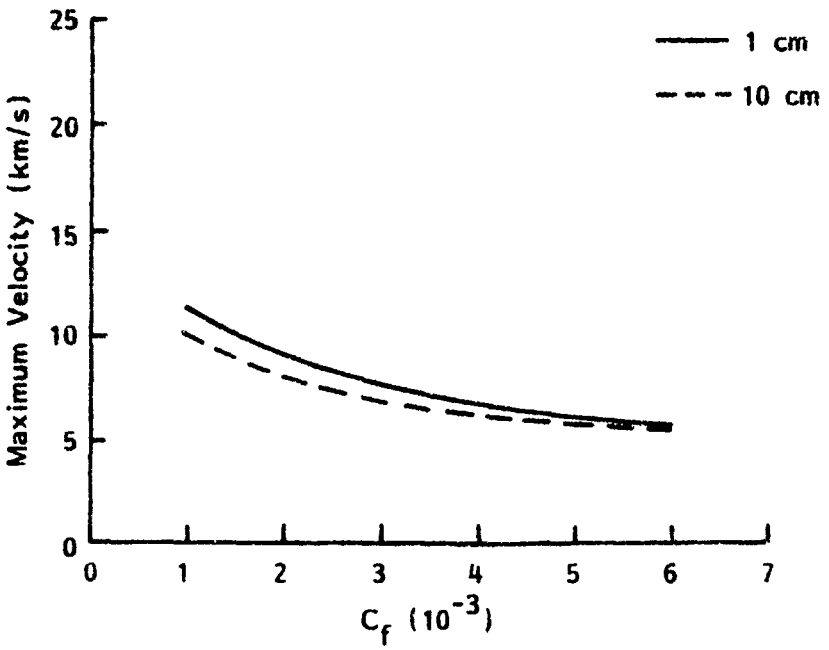

Figure 7. Maximum Velocity as a Function of the Skin Friction Coefficient for the Transitioning Armature

in the range from 10 to 30 V per anode/cathode pair, Reference 12. To determine how smaller values of the contact potential might affect performance predictions, we investigated two other muzzle voltage scaling relationships corresponding to values of the contact potential drop, V_c, of 50 V and 0 V. Again, the scaling law was based on Equation (5) with experimentally measured muzzle voltages for SSG and small-bore guns used to determine the constants V_b' and α. In this manner, we find that $V_b' = 860\ V/m^{\alpha}$ and $\alpha = 0.46$ for $V_c = 50$ V, and $V_b' = 790\ V/m^{\alpha}$ and $\alpha = 0.35$ for $V_c = 0$. A comparison of the voltages predicted by the three scaling relations is shown graphically, for the plasma armature, in Figure 8. In the bore dimension range of present interest, the muzzle voltage curves do not deviate significantly from one another. Consequently, the armature efficiency curves, shown in Figure 9 as a function of M_p for hybrid and transitioning armatures operating at 7.5 km/s, are essentially indistinguishable for the three voltage scaling relationships. We would expect the efficiency of the hybrid armature to be somewhat more sensitive than the plasma armature to the voltage scaling relation since, for the hybrid, the armature voltage drop is dominated by V_c. Nonetheless, even for the hybrid the efficiency is relatively insensitive to the voltage scaling relationship, primarily because the dominant loss mechanism in the hybrid armature is the armature parasitic mass.

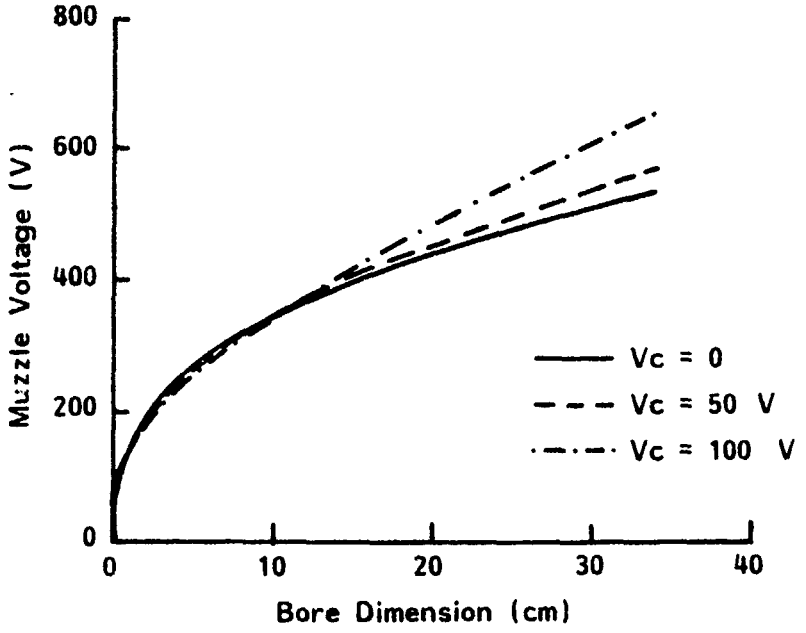

Figure 8. Comparison of Voltage Scaling Relationships

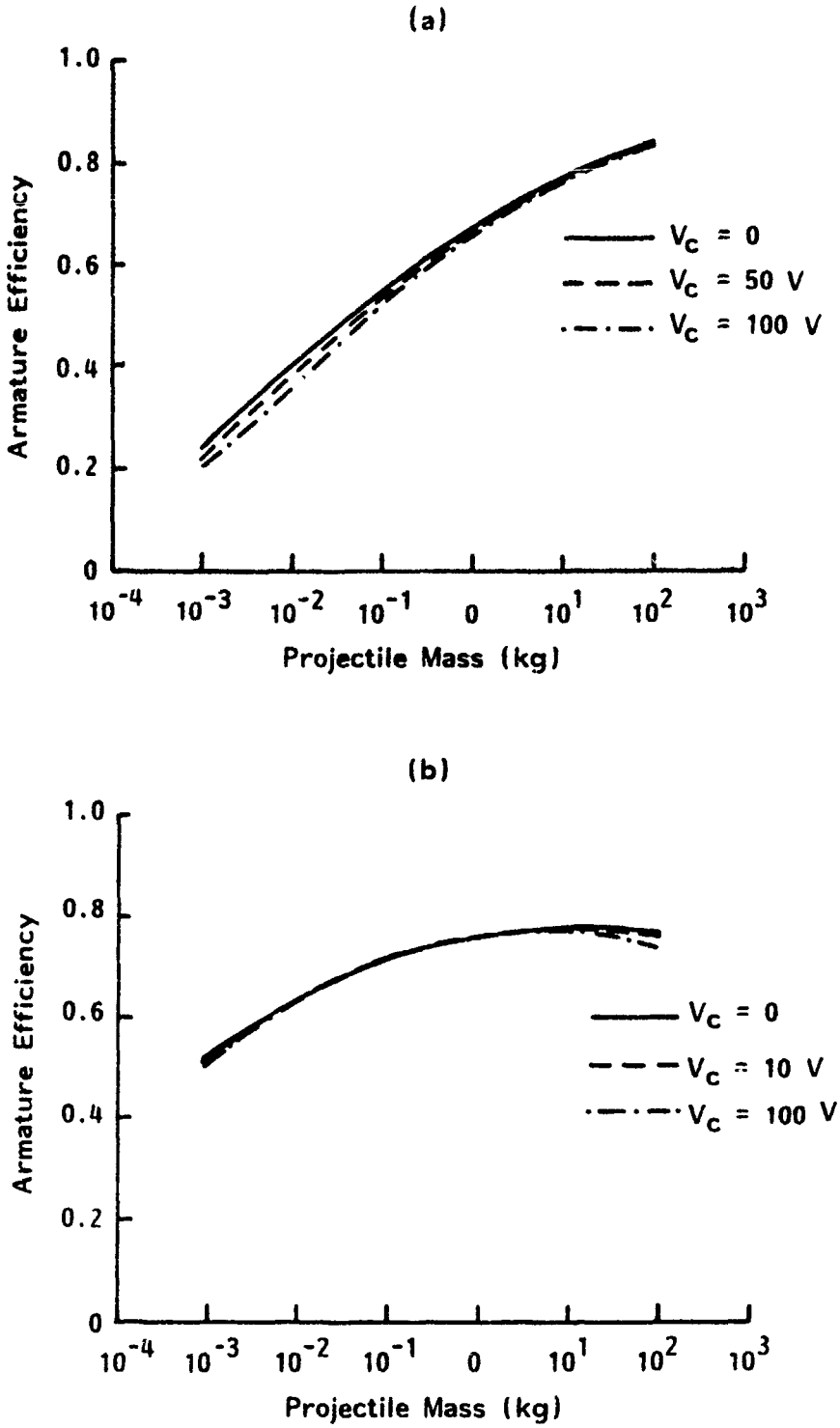

Figure 9. Effect of Voltage Scaling on Armature Efficiency for (a) Hybrid and (b) Transitioning Armatures (v = 7.5 km/s)

SECTION V
CONCLUSIONS

We have developed a model for investigating armature performance as a function of railgun geometry, armature type, and gun operating conditions. Two key figures of merit are established for evaluating a particular armature – the armature efficiency, η, and the maximum velocity, v_{max}. The armature efficiency corresponds to the ratio of the increase in kinetic energy to the energy provided to the launch package during acceleration, while v_{max} represents the maximum velocity that can be achieved for a given set of bore geometry and materials, projectile characteristics, and current level. The model, which can be used to study all four major armature types (solid, plasma, transitioning, and hybrid armatures), accounts for the effects, on armature performance, of parisitic mass, armature resistance, friction, ablation drag, and, for the hybrid armature, gap growth. The model can be used to identify the dominant loss mechanisms for each type of armature, to provide a relative ranking of the armatures based on efficiency and maximum velocity for a particular application, and to guide experimental efforts by providing a framework for assessing the sensitivity of performance predictions to parameters that are not yet well defined. It is intended that the model be updated on a regular basis to reflect the progress made in understanding the loss mechanisms described here, as well as additional performance degrading phenomena, such as restrike, blowby, and armature instabilities, which, at present, are poorly understood.

In this paper, we used the armature model to determine how η and v_{max} scale with projectile mass (and correspondingly bore size) and with j, the current per unit rail height. We restricted consideration to the hypervelocity regime (v greater than 7 km/s), so that we evaluated only the plasma, transitioning, and hybrid armatures. Furthermore, since, in this regime, the transitioning and plasma armatures exhibit similar trends, with the transitioning armature having slightly higher values of η and v_{max}, our discussion here will focus on the transitioning and hybrid armatures.

For the specific conditions considered in this analysis and a projectile muzzle velocity of 7.5 km/s, we derive the following conclusions regarding armature efficiency. The efficiency of the transitioning armature increases

with projectile mass, from a value of 0.5 for gram-sized projectiles to a broad maximum of 0.8 for kilogram-sized projectiles. This increase in efficiency with projectile mass is derived primarily from our voltage scaling relation which predicts that the voltage increases with bore dimension with some power less than unity. The efficiency of the hybrid armature also increases with projectile mass. Although the hybrid armature's efficiency is less than that of the transitioning armature for small masses, it becomes comparable to that of the transitioning armature for kilogram-sized projectiles. The increase in efficiency with projectile mass for the hybrid armature is a direct result of the favorable scaling of the parasitic mass ratio with projectile mass. For both transitioning and hybrid armatures, the efficiency is relatively insensitive to j for values between 2×10^7 and 4×10^7 A/m.

For the conditions studied here, the velocity limit for the hybrid armature exceeds 15 km/s, the highest muzzle velocity investigated in our study. On the other hand, ablation drag and viscous drag limit the velocity to less than 10 km/s for the transitioning armature. It is interesting to note that v_{max} for the transitioning armature does not exhibit the same favorable scaling with projectile mass that η does. The scaling of v_{max} with j is not straightforward because of the competition between opposing trends. As the current increases, the energy dissipated in the armature and transferred to the bore during acceleration decreases, but this energy is more effective in causing ablation.

Our calculations suggest that we may have some flexibility in extending v_{max} by altering the gun operating conditions. For example, Figure 10 shows the maximum velocity as well as the efficiency for a transitioning armature accelerating a low-mass projectile in a 10-cm bore gun. The projectile mass of 250 g, used to generate the curves in Figure 10, is an order of magnitude lower than the nominal mass for the 10-cm gun as determined by Equation (16). Comparison of Figure 10 with Figure 4 shows that the maximum velocity for the low-mass projectile is approximately a factor of two higher than that for the nominal mass at a current per unit rail height of 4×10^7 A/m. Of course, a reduction of an order of magnitude in projectile mass, at the same current level, leads to an order of magnitude increase in acceleration, which presents a challenge to projectile design.

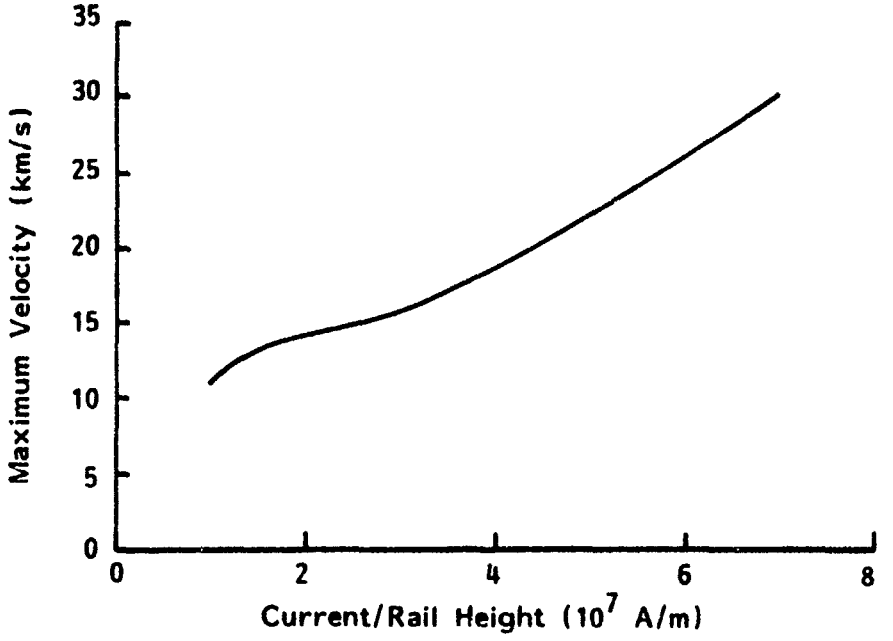

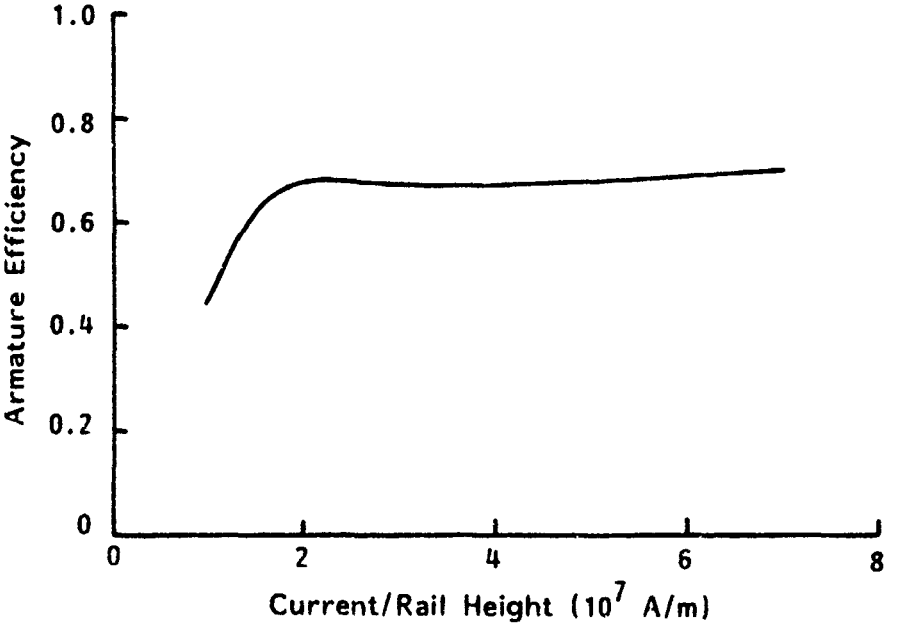

Figure 10. Maximum Velocity and Efficiency for a Transitioning Armature Accelerating a 250-gram Projectile in a 10-cm Bore Gun

It is necessary to keep in mind that the values of several parameters used in this analysis, and their variation with gun geometry and operating conditions, are not yet well defined. This uncertainty applies particularly to the parameters which define the ablation drag and voltage scaling, and to the armature friction coefficient. Until more accurate values become available, one must proceed cautiously in quantitatively interpreting our results, particularly when the scaling analyses extend beyond the regimes where experimental data is available. Indeed one of the principal uses of the armature model is to determine the sensitivity of the model's predictions of armature performance to parameters which are not well defined in order to guide future experimental efforts.

For example, our simulations indicate that the maximum velocity which can be achieved with the transitioning and plasma armatures, although relatively insensitive to the entrainment fraction for values of f_R and f_D between 0.5 and 1, is highly sensitive for values below about 0.2. Likewise, the predicted maximum velocity is highly sensitive to the friction coefficient for values of C_f below about 0.003. Our predictions of armature performance are relatively insensitive to the value of the contact potential primarily because we fit the parameters in our voltage scaling relationship so that the curves will pass through the representative values taken for a one-centimeter and ten-centimeter bore gun. On the other hand, our scaling neglects any explicit dependence of voltage on current, which could significantly alter these conclusions. Clearly, additional information on the scaling of the physical parameters which control ablation drag, friction, and armature voltage drop are necessary to more accurately assess armature performance.

APPENDIX A

DERIVATION OF THERMAL CONDUCTION PARAMETERS FOR ABLATION DRAG AND GAP GROWTH

APPENDIX A

DERIVATION OF THERMAL CONDUCTION PARAMETERS FOR ABLATION DRAG AND GAP GROWTH

A fraction of the energy incident on the rails and dielectrics is lost to conduction and does not lead directly to bore ablation. Schnurr and Kerrisk, Reference 13, have developed an approximate expression for the heat lost to conduction, based on the assumption that the time required for the bore surface to be raised to the vaporization temperature is small compared to the arc transit time. While this assumption is valid for typical dielectric materials, such as lexan, even for velocities on the order of 15 km/s, it is generally not valid for rail materials or ceramic insulators for velocities greater than a few kilometers per second. In this Appendix, we extend the analysis of Schnurr and Kerrisk to account for the time required to raise the surface temperature to the vaporization temperature. We consider only the rail surface, since the procedure for calculating the heat lost to the dielectrics is identical except for the change in thermophysical properties.

Based on a comparison of analytic solutions with detailed numerical computations, Schnurr and Kerrisk suggest that the power per unit area lost to conduction , q_L, for a point on an ablating rail can be approximated simply by the power flux conducted into a surface whose surface temperature is instantaneously raised to the vaporization temperature, T_{vR}, and then held constant at that value, namely

$$q_L\ (t_e) = \frac{k_{LR}\ (T_{vR} - T_i)}{[\pi \alpha_{LR}\ t_e]^{\frac{1}{2}}} \qquad \text{(A-1)}$$

where k_{LR} and α_{LR} are the thermal conductivity and thermal diffusivity, respectively, of the molten rail material, T_i is the initial temperature of the rail, and t_e, the exposure time, represents the time since the surface was raised to T_{vR}. Of course, Equation (A-1) is valid only during the transit time of the armature.

In reality, the rail surface is not raised to T_{vR} instantaneously. Indeed, if we assume that the point in question is subject to a constant power

flux, q_R, then it will first reach the vaporization temperature at the time, Reference 14

$$t_v = \frac{\pi}{\bar{\alpha}_R} \left[\frac{\bar{k}_R (T_{vR} - T_i)}{2q_R} \right]^2 \qquad \text{(A-2)}$$

where the overbar denotes representative values of the thermophysical properties in the temperature range T_i to T_{vR}. The power flux, q_R, is related to the heat flux, Q_R, in Equation (4) by $q_R = Q_R/2h\ell$. Until time t_v, no ablation is assumed to occur, and all the incident flux, that is q_R, is taken to be lost to conduction into the rail material.

For $t>t_v$ but less than the arc transit time, t_t, we use the Schnurr-Kerrisk approximation to calculate the heat lost to conduction. However, since the surface has been gradually raised to the vaporization temperature, we adjust the exposure time such that the heat lost to conduction is continuous at $t=t_v$. In other words, we use Equation (A-1) for q_L, but replace t_e by $t_e-\tau$ where τ is determined by requiring q_L at $t_e=t_v$ to be equal to q_R. This condition leads to the expression

$$\tau = t_v (1-\lambda_R) \qquad \text{(A-3)}$$

where

$$\lambda_R = \frac{4}{\pi^2} \left[\frac{\bar{\alpha}_R}{\alpha_{LR}} \right] \left[\frac{k_{LR}}{\bar{k}_R} \right]^2 . \qquad \text{(A-4)}$$

Accordingly, q_L for $t > t_v$ can be written as

$$q_L = q_R \left[\lambda_R t_v/(t_e-\tau)\right]^{\frac{1}{2}} . \qquad \text{(A-5)}$$

If we assume that the arc length, ℓ, and armature/projectile velocity, v, are constant during the arc transit time, we can express the exposure time for any point on the rail located at a distance ξ from the back of the projectile as

$$t_e = \frac{\xi}{v} . \qquad \text{(A-6)}$$

Thus, at any time, t, the power per unit area lost to conduction into the rails can be written as

$$q_L(\xi) = \begin{cases} q_R & , \quad 0 \le \xi \le x_v \\ q_R \left[\dfrac{\lambda_R x_v}{\xi - x_v (1-\lambda_R)} \right]^{1/2} & , \quad x_v \le \xi \le \ell \\ 0 & , \quad \xi > \ell \end{cases} \tag{A-7}$$

where $x_v = v\, t_v$.

If we define β_R to be the fraction of the thermal power incident on the rail surface which leads to ablation, then

$$\beta_R = 1 - \frac{1}{q_R \ell} \int_0^{\ell'} q_L(\xi)\, d\xi \, . \tag{A-8}$$

Carrying out the integration, we obtain the following expression for β_R:

$$\beta_R = 1 - \frac{x_v}{\ell} - 2 \left(\lambda_R \frac{x_v}{\ell} \right)^{1/2} \left[\left[1 - \frac{x_v}{\ell} (1 - \lambda_R) \right]^{1/2} - \left[\lambda_R \frac{x_v}{\ell} \right]^{1/2} \right] . \tag{A-9}$$

For the hybrid armature we must account for the ablation of the solid part of the armature. Since the surface of the solid armature remains in contact with the plasma throughout the acceleration period, we do not have to consider motion of the plasma relative to the solid surface; however, we account for the heat that is lost to conduction into the solid armature, q_{Ls}. This heat loss is given by

$$q_{Ls} = \frac{\bar{k}_s (T_{vs} - T_i)}{(\pi \bar{\alpha}_s t_s)^{1/2}} \tag{A-10}$$

where $\bar{k}_s$ is the representative value of thermal conductivity of the solid armature, $\bar{\alpha}_s$ its representative thermal diffusivity, T_{vs} its vapor temperature, and T_i its initial temperature. Also, in this equation, t_s is the time since the surface of the solid armature reached its vapor temperature. Because the plasma and the solid armature surface remain in contact throughout the acceleration period, we assume that the solid armature surface reaches the vaporization temperature instantly and, therefore, t_s is set equal to t, the acceleration time.

The fraction, β_s, of the heat flux to the solid armature, q_s, that actually leads to ablation is given by

$$\beta_s = 1 - \frac{q_{Ls}}{q_s} \quad . \tag{A-11}$$

The heat flux, q_s, can be written as

$$q_s = \left[\frac{IV + vF_D}{4h\ell}\right]$$

This fraction may also be written as

$$\beta_s = 1 - \left[\frac{t_{vs}}{t}\right]^{1/2} \tag{A-12}$$

where

$$t_{vs} = \frac{4}{\pi\alpha_s}\left[\frac{\bar{k}_s\,(T_{vs} - T_i)}{2q_s}\right]^2 \tag{A-13}$$

is a characteristic conduction time for the solid armature.

APPENDIX B

DERIVATION OF PARASITIC MASS FOR HYBRID ARMATURES

APPENDIX B

DERIVATION OF PARASITIC MASS FOR HYBRID ARMATURES

The mass of a conductor required to carry a current, I, for a time, t, without melting can be derived from the heat equation. For the solid armature we have

$$\rho_s C_p \frac{dT}{dt} = \frac{I^2 R}{V_s} = \frac{I^2 \eta_{rs}}{V_s h} \qquad \text{(B-1)}$$

where ρ_s is the density of the solid conductor, C_p is its specific heat, T is the conductor temperature, assumed to be uniform throughout the conductor, R is the conductor resistance, η_{rs} is its resistivity, and V_s is the volume occupied by the conductor. In deriving this equation we have assumed that energy is deposited in the conductor uniformly and that the only source for this energy is ohmic heating. Also, we have assumed that no heat is lost from the conductor by thermal conduction.

After integrating Equation (B-1) we obtain an expression for the conductor mass, M_c, required to carry the current, I, for a time, t, given by

$$M_c = hI\sqrt{t/\gamma} \qquad \text{(B-2)}$$

where γ, a parameter which is related to the action constant of the conductor, is given by

$$\gamma = \frac{1}{\rho_s} \int_{T_i}^{T_f} \frac{C_p}{\eta_{rs}} \, dT \, . \qquad \text{(B-3)}$$

In Equation (B-3), T_i is the initial temperature of the conductor and T_f is its allowed final temperature (the melt temperature in this case).

In some solid armature designs, the solid armature is made up of metal conductors imbedded in a composite matrix to insure a more uniform distribution of current in the armature. To account for the additional mass of the matrix we introduce the ratio of the armature mass to conductor mass, f_{ac}, into Equation

(B-2) and obtain an expression for the solid armature mass, M_{sa}, given by

$$M_{sa} = f_{ac}\, hI \sqrt{t/\gamma} \quad . \tag{B-4}$$

A limiting case, analytical solution can be obtained for the solid armature mass necessary to accelerate a projectile of mass, M_p, to a given velocity, v_f, if we assume friction drag and ablation drag are negligible. With these two assumptions, Equation (1) can be integrated to obtain

$$v_f - v_i = \frac{L'I^2}{2(M_p + M_{sa})}\, t \quad . \tag{B-5}$$

where v_i is the initial projectile velocity and t is the time required to accelerate the projectile to velocity v_f.

After solving Equation (B-4) for the acceleration time, t, and substituting this time into Equation (B-5), we obtain a quadratic equation for M_{sa}. This equation may then be solved for M_{sa}/M_p giving

$$\frac{M_{sa}}{M_p} = \lambda\, (1 + \sqrt{1 + 2/\lambda}) \tag{B-6}$$

where

$$\lambda = \frac{f_{ac}^{\,2}\, h^2 (v_f - v_i)}{\gamma L' M_p}$$

The armature mass predicted by Equation (B-6) was found to agree very well with that predicted by our numerical calculations. The good agreement is due to the fact that skin friction effects and ablation effects do not significantly alter the acceleration time from that predicted by Equation (B-5).

APPENDIX C

ANALYTIC SOLUTION FOR ARMATURE EFFICIENCY

APPENDIX C

ANALYTIC SOLUTION FOR ARMATURE EFFICIENCY

As a means of analytically checking our armature efficiency calculations we consider the Case 2 calculations which include the efficiency losses due to the initial parasitic mass and the armature resistance. For this case the efficiency may be expressed as

$$\eta_2 = \frac{KE_p}{KE_{tot} + E_{ohmic}} \tag{C-1}$$

where KE_p is the increase in kinetic energy of the projectile, KE_{tot} is the increase in kinetic energy of the projectile/armature package, and E_{ohmic} is the energy ohmically dissipated in the armature. These quantities may be individually expressed in terms of the following equations.

$$KE_p = \frac{L'I^2x_f}{2} \left[\frac{M_p}{M_a + M_p} \right] \tag{C-2}$$

$$KE_{tot} = \frac{L'I^2x_f}{2} \tag{C-3}$$

and

$$E_{OHMIC} = IVt_f \ . \tag{C-4}$$

In these expressions t_f is the total acceleration time and x_f is the barrel length.

For Case 2, the acceleration

$$a = \frac{L'I^2}{2(M_a + M_p)} \tag{C-5}$$

is constant so that t_f and x_f can be expressed simply in terms of the initial velocity, v_i, and the final velocity, v_f, as

$$t_f = \frac{(v_f - v_i)}{a} \tag{C-6}$$

and

$$x_F = \frac{\left(v_f^2 - v_i^2\right)}{2a}, \tag{C-7}$$

respectively. After substitution we obtain the analytic expression for the Case 2 efficiency as

$$\eta_2 = \frac{1}{\left(1 + \frac{M_a}{M_p}\right)\left(1 + \frac{4\,V}{L'I\,(v_f + v_i)}\right)} \tag{C-8}$$

The efficiency predicted by Equation (C-8), provides an accurate estimate for the efficiency for the hybrid armature since the losses in the hybrid arise primarily from the parasitic mass of the solid conductor and the voltage drop in the brushes.

REFERENCES

1. L.D. Thornhill, J.H. Batteh, and J.L. Brown, "Armature Options for Hypervelocity Railguns," Proc. of the Fourth Electromagnetic Launch Symposium, Austin, TX, in press.

2. J.V. Parker, W.M. Parsons, C.E. Cummings, and W.E. Fox, "Performance Loss due to wall ablation in plasma armature rail guns," in AIAA Fluid Dynamics and Plasma Dynamics and Lasers Conference, Paper AIAA-85-1575, July, 1985.

3. K.A. Jamison, "Diagnostics of Plasma Armatures," Proc. of the First EM Gun Armature Workshop (Air Force Armament Laboratory, Eglin AFB, FL), June, 1986.

4. R. Dethlefsen, E. Waisman, E. Kennedy, and R. Puterbaugh, "Advanced Armature Program, Task I, Armature Survey and Models," AFATL-TR-88-56, September, 1988.

5. M.M. Holland, P.D. Eggers, J.R. German, A.P. Krickhuhn, F.E. LeVine, T.E. McKelvey, P. Riedy, J. Thurman, and G.M. Wilkinson, "EMGWS Task B Single Shot Gun," Proc. of the Fourth Electromagnetic Launch Symposium, Austin, TX, in press.

6. J.H. Batteh, "Arc-Dynamic Calculations in the Rail Gun," BRL contract report ARBRL-CR-00521, 1983.

7. K.A. Jamison, H.S. Burden, and J.D. Powell, "Plasma Properties of a Large-Bore, Arc-Armature Railgun," BRL report, in press.

8. K.A. Jamison and H.S. Burden, "Measurements of Plasma Properties from a Large Bore, Plasma Armature Railgun," Proc. of the Fourth Electromagnetic Launch Symposium, Austin, TX, in press.

9. J.D. Powell, "Plasma Analysis of a Large-Bore, Arc-Driven Railgun," Proc of the Fourth Electromagnetic Launch Symposium, Austin, TX, in press.

10. D. Kulhmann-Wilsdorf and J.H. Cuadros, "Capabilities of Metal Fiber Brushes with Plastic Contact Spots for High-Speed/High Current Density Applications," Proc. of the First EM Gun Armature Workshop (Air Force Armament Laboratory, Eglin AFB, FL), June, 1986.

11. R.S. Hawke, A.L. Brooks, C.M. Fowler, and D.R. Peterson, "Electromagnetic Railgun Launchers: Direct Launch Feasibility," AIAA Journal, Vol. 20, No. 7, pp. 978-985, July, 1982.

12. J. Cobine, Gaseous Conductors, Chap. 9, Dover Publications, Inc., New York, 1958.

13. N.M. Schnurr and J.F. Kerrisk, "Numerical Studies of ablation and Ionization of Railgun Materials," in AIAA Fluid Dynamics and Plasma Dynamics and Lasers Conference, Paper AIAA-85-1576, July, 1985.

14. P.J. Schneider, "Conduction," in Handbook of Heat Transfer, edited by W.M. Rohsenow and J.P. Hartnett (McGraw Hill, New York, 1973).